Semiconductor Physics, Quantum Electronics & Optoelectronics, 2013. V. 16, N 1. P. 48-54.

PACS 66.H-, 71.15.-m, 71.20.-b

Electron structure of the equilibrium and metastable phases in superionic Li_2SiS_3

D.I. Bletskan, V.V. Vakulchak, K.E. Glukhov, O.A. Mykaylo
Uzhhorod National University, Physics Faculty, 46, Pidhirna str. 88000 Uzhhorod, Ukraine
Phone/fax: +38(031)-223-73-67; *e-mail*: *crystal_lab457@yahoo.com*

Abstract. The calculations of a band structure $E(k)$, the total $N(E)$ and partial densities of electron states, as well as spatial distribution of the valence charge $\rho(r)$ for the equilibrium (*e*) and metastable (*m*) phases of superionic Li_2SiS_3 were performed in a local approximation of the density functional theory (DFT) from the first principles for pseudopotentials in the basis of numerical pseudoatomic orbitals. The total density of states in the valence band calculated all over the Brillouin zone for both crystalline phases Li_2SiS_3 was compared to the experimental X-ray photoelectron spectra of the equilibrium, metastable and glassy phases. It is a good agreement between the calculation and experimental results for all bands of crystalline and glassy phases.

Keywords: superionics, lithium silicon sulfide, band structure, density of states, electron charge density map.

Manuscript received 07.11.12; revised version received 05.12.12; accepted for publication 26.01.13; published online 28.02.13.

1. Introduction

In Li_2S-SiS_2 system, two ternary compounds were found to exist: Li_2SiS_3, melting congruently at T_m = 1018 ± 10 K, and Li_4SiS_4, melting incongruently at T_m = 983 ± 20 K [1, 2]. Li_2SiS_3 and Li_4SiS_4 ternary compounds are obtained by direct co-melting of Li_2S and SiS_2 compounds in the ratio 1:1 and 2:1, respectively, in pre-evacuated sealed graphitized silica ampoules at temperatures not exceeding 1273 K [1, 2]. Depending on the melt cooling conditions, either an equilibrium phase, or the metastable crystalline one, or glassy Li_2SiS_3 can be obtained. The equilibrium crystalline phase is obtained upon rapid cooling to 993 K with subsequent annealing at the same temperature. The metastable phase is obtained under slow melt cooling from T_m down to the room temperature for 5-6 hours. By melt quenching from 1053 K into water or liquid nitrogen, one can obtain glassy Li_2SiS_3. The glass-transition and crystallization temperatures of Li_2SiS_3 are T_g = 593 K and T_c = 723 K, respectively [1].

In spite of the available data regarding structural studies of both crystalline phases [1, 3] and glassy Li_2SiS_3 by the direct techniques of X-ray [4] and neutron diffraction [5, 6] as well as vibrational spectroscopy [7, 8] and nuclear magnetic resonance [9, 10], physical properties of this compound have been studied quite poorly. Detailed investigations of the ionic conductivity were performed for both crystalline phases [1, 3] as well as stoichiometric [1] and non-stoichiometric glasses [9], also modified with LiI [11], LiBr [12], Li_2PO_4 [13, 14]. Analysis of the available experimental data on Li_2SiS_3 conductivity shows the electrical conductivity to increase by two orders of magnitude at the transition from the crystalline to glassy state, which is not typical for classical binary glass-forming compounds like $GeSe_2$, As_2S_3, As_2Se_3. For these compounds, the crystal-glass transition is accompanied by a decrease in electrical conductivity by one or two orders [15]. From the practical viewpoint, the existence of the high ionic conductivity ($1\cdot10^{-4}$ Ω^{-1} cm^{-1}) in glassy Li_2SiS_3 [1] is very important, and its value can be increased by an

incorporation of LiI [11], LiBr [12], or Li_2PO_4 [13, 14] modifiers. It is the high ionic conductivity that makes lithium-containing silicon sulfide glasses (glassy silicon sulfides) promising solid electrolytes for lithium-ion batteries [11] and causes an increased interest towards these glasses.

With regard to the optical properties and theoretical calculations of the electron structure of the equilibrium and metastable crystalline phases Li_2SiS_3, such studies have not been carried out before. In this work, we report on the density functional theory (DFT) calculations of electron energy structure, the total $N(E)$ and partial densities of electron states for the equilibrium and metastable phases Li_2SiS_3, as well as the spatial distribution of valence charges in the unit cells of these modifications. The calculations of the total density of states $N(E)$ were compared with the available data of X-ray photoelectron spectra (XPS) for the crystals of both phases and the glassy Li_2SiS_3.

2. Crystal structure of the equilibrium and metastable phases of Li_2SiS_3

The equilibrium phase Li_2SiS_3 (*e*) is isostructural to Li_2SiO_3 [16] and crystallizes in an orthorhombic lattice with the parameters a = 11.664 Å, b = 6.735 Å, and c = 5.926 Å, $Cmc2_1$ space group [1, 3]. The crystal structure of the equilibrium phase and its projection on the YZ plane are shown in Figs 1a and 1b, respectively. The unit cell contains four formula units (Fig. 2). Its volume is 466 $Å^3$, and the theoretically calculated density is 1.97 g/cm^3. Experimental measurements of the density for a slowly cooled sample gave the value of 1.87 g/cm^3 [5]. The main structural elements of Li_2SiS_3 crystal structure are $[SiS_4]$ tetrahedra linked by common vertices in infinite zigzag chains extending along the c axis (Fig. 1b). Each subsequent $[SiS_4]$ tetrahedron in the chain is turned by 180° with respect to the previous one. Parallel infinite chains are linked together by weak Van der Waals forces, Li^+ ions being located in the Van der Waals space. The Si–S–Si valence bond angles are between 138° and 143°. Eight lithium ions are located in interstitial sites surrounded by five sulfur ions. As noted in Ref. [1], there are two types of sixfold interstitial sites in Li_2SiS_3 structure, differing in the shape of octahedra and their occupation by lithium ions. An important element of Li_2SiS_3 crystal structure is the presence of octahedral interstitial sites forming conductive "tunnels" along the c axis that provide the conducting channels along which lithium ions move under an external electric field. This factor determines a rather high ionic conductivity value in this phase.

The metastable crystalline phase Li_2SiS_3 (*m*) also possesses orthorhombic structure typical for the equilibrium one, but with different lattice parameters: a = 11.436 Å, b = 6.605 Å, and c = 6.487 Å [1]. The comparison of crystal lattice parameters for the equilibrium and metastable phases shows that the a and b parameters of the metastable phase are smaller than the same parameters of the equilibrium one. On the other hand, the c parameter is greater in the metastable phase than in the equilibrium one. Consequently, the chains of vertex-linked $[SiS_4]$ tetrahedra in the metastable phase are more elongated along the c axis than in the equilibrium phase, so that a and b lattice parameters decrease, but the c parameter and the valence bond angle Si–S–Si increase. Besides, the unit cell volume increases by 5%.

3. Calculation method

The calculations of the energy band structure were carried out within the framework of the density functional theory [17, 18] in the local approximation for the account of exchange and correlation effects [19, 20], using SIESTA software [21, 22]. Linear combinations of atomic orbitals were used as a fundamental calculation basis. The periodic structure of crystal is taken into

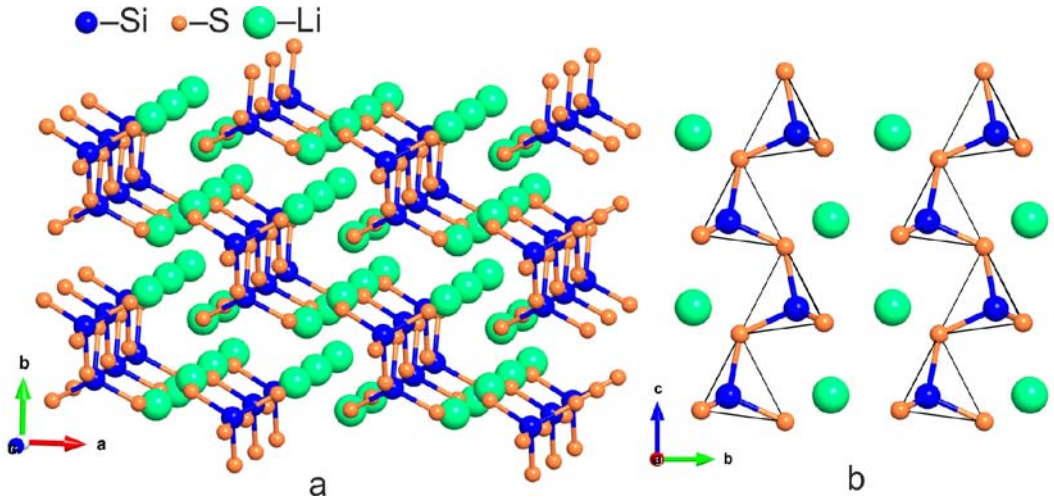

Fig. 1. The crystal structure (*a*) and its projection on the XZ plane (*b*) for the equilibrium phase of Li_2SiS_3.

Table. Parameters of the band spectrum for the equilibrium and metastable phases in Li_2SiS_3.

Compound	E_{VB}, eV	k_V	k_C	E_{gi}, eV	E_{gd}, eV	E_{VB1}, eV	E_{VB2}, eV	E_{VB3}, eV	E_{VB4}, eV	ΔE_1, eV	ΔE_2, eV	ΔE_3, eV	E_{CB1}, eV
Li_2SiS_3(e)	13.83	Z	G→F	2.82	2.99	2.41	2.26	2.02	2.69	0.19	0.55	3.79	0.98
Li_2SiS_3(m)	13.4	F	G→F	2.52	2.67	2.08	2.19	1.92	2.34	0.26	0.75	3.86	1.29

account through the boundary conditions at the unit cell boundaries. First-principle atomic norm-preserving pseudopotentials [23, 24] for electron configurations of Si ([Ne] $3s^23p^2$) and S ([Ne] $3s^23p^4$) atoms were used in the calculations. These states belong to the valence shells while [Ne] is related to the core.

The plane wave effective cutoff energy E_{cut} = 200 Ry for the self-consistent calculation (SCF) was chosen in such a way to obtain cell energy convergence not worse than 0.001 Ry/atom. Then the basis contained about 30500 atomic orbitals. The density of *k*-points mesh in the reciprocal space for the self-consistent calculation was chosen from the same reason. The electron density was calculated by interpolation between the nodes of 5×5×6 grid in the reciprocal space. The total and partial densities of electron states were determined by the modified tetrahedra method, for which the energy spectrum and wave functions were calculated on a *k*-grid containing 75 points. Integration over the irreducible part of the Brillouin zone was performed using the method of special *k*-points [25, 26].

4. Results and discussion

4.1. Band structure and the nature of electron states

The band structure calculation was performed for the high symmetry points and directions in the Brillouin zone shown in Fig. 3.

The band structure of the equilibrium and metastable crystalline phases of Li_2SiS_3 calculated without spin-orbit interaction is presented in Fig. 4. The base energy corresponds to the highest occupied state. The energy band structures of the two phases are qualitatively similar to each other and have characteristic topology with four clearly separated energy regions possessing a "doublet" structure. The valence bands of both crystals possess weak dispersion and form separate energy subbands (VBI, VBII, VBIII, VBIV) that correspond to distinct maxima in $N(E)$ (Fig. 5). The main quantitative parameters of the electron spectra for both crystal structures of Li_2SiS_3 are presented in Table. We used the following notations in the table: E_{VB} is the total valence band width, k_V is the point of the Brillouin zone corresponding to the valence band maximum, k_C is the bottom of the lower unoccupied band, E_{VB1}, E_{VB2}, E_{VB3}, and E_{VB4} are the widths of allowed energy bands for the first, second, third, and fourth subbands of the valence band, numbering the bands started from the top, ΔE_1, ΔE_2, and ΔE_3 are the energy gap bandwidth, E_{CB1} is the width of the lower unoccupied subband, E_{gi} is the indirect band gap, E_{gd} is the direct band gap.

The top of the valence band (the absolute maximum) of the equilibrium Li_2SiS_3 is in the Z point, and for the metastable phase it is in the vertex point F of the Brillouin zone. The bottom of the conduction band (absolute minimum) in both phases is not in a high-symmetry point, but at the Brillouin zone edge in the direction G-F at the distance of ca. 1/3 from the G point. The band extrema have the following coordinates in the basic reciprocal lattice vector units: Z (0, 0, 1/2), F (1/3, 1/3, 0), G (1/3, 1/3, 1/2). Consequently, both Li_2SiS_3 crystals are indirect-gap superionic semiconductors with calculated indirect band gap E_{gi} = 2.82 eV for the equilibrium phase of Li_2SiS_3 and E_{gi} = 2.52 eV for the metastable one. It should be noted that the calculations in the local density approximation within the framework of the density functional theory always give underestimated band gap values.

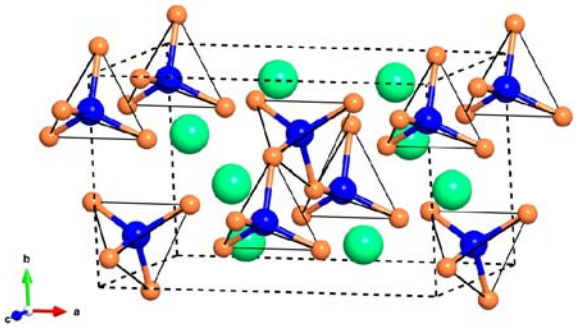

Fig. 2. The unit cell of the Li_2SiS_3 equilibrium phase.

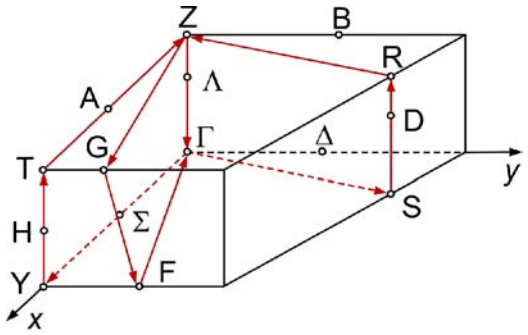

Fig. 3. The Brillouin zone of orthorhombic Li_2SiS_3 ($Cmc2_1$).

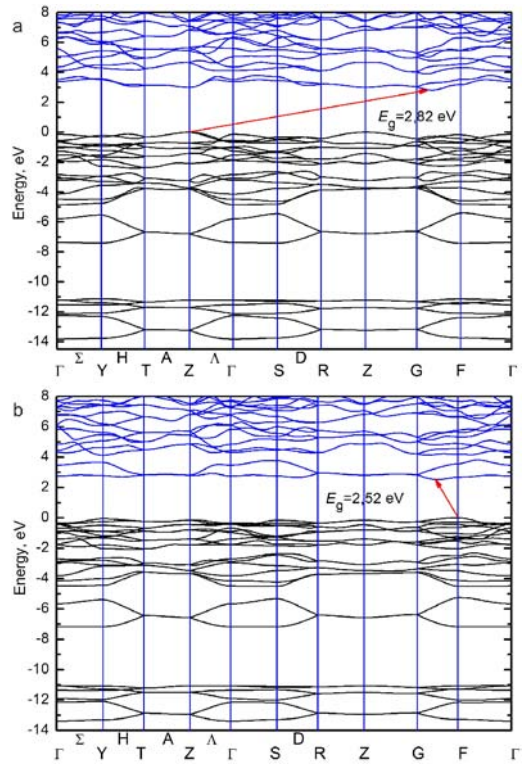

Fig. 4. The band structure of the equilibrium orthorhombic (*a*) and metastable (*b*) phases in Li_2SiS_3 ($Cmc2_1$).

Calculations of the total $N(E)$ and partial densities of electron states provide information on the contribution of atomic orbitals into the crystalline states, which for both modifications of Li_2SiS_3 are qualitatively similar (Fig. 5). The main contribution to the valence band in both crystalline phases is made by *s*- and *p*-states of sulfur. The analysis of the total and partial densities of electron states for both crystals shows that the lowest valence subband VBIV is formed predominantly by 3*s*-states of sulfur with a small admixture of 3*s*- and 3*p*-states of silicon and 2*p*-states of lithium. The VBIII subband is formed by roughly equal similar contribution of hybridized Si 3*s*- and S 3*p*-states.

3*p*-orbitals of sulfur mixed with 3*p*-orbitals of silicon and 2*s*- and 2*p*-states of lithium are mostly involved in the formation of the VBII subband. Finally, 3*p*-orbitals of sulfur with a small admixture of 3*d*-states of silicon and 2*s*- and 2*p*-states of lithium make the main contribution to the topmost valence VBI subband.

The lowest unoccupied CBI subband is separated from other unoccupied bands by a gap. The lower conduction band is characterized by hybridization of all silicon states with 3*p*- and 3*d*-states of sulfur as well as 2*s*- and 2*p*-states of lithium. The resulting position of individual energy subbands of silicon, sulfur and lithium in Li_2SiS_3 can be explained by the preserved atomic genesis of these subbands with account of effective charges on atoms in the crystal. A higher electronegativity of S atoms compared to the Si ones leads to the smaller binding energies for the *s*- and *p*-states of sulfur, thus determining the relative positions of S and Si subbands in the valence band of Li_2SiS_3. From this assumption on the reasons for the relative positions of the Si and S subbands in the valence band Li_2SiS_3, it follows directly that the fraction of ionicity in the Si–S chemical bond is quite substantial.

X-ray photoelectron spectroscopy (XPS) is an informative experimental technique for studying the electron structure of crystalline and glassy superionics. For both crystalline phases and glassy Li_2SiS_3 experimental X-ray photoelectron spectra are available, which provide information on the energy distribution of electron states in the valence band. Comparison of the theoretically calculated total and partial densities of

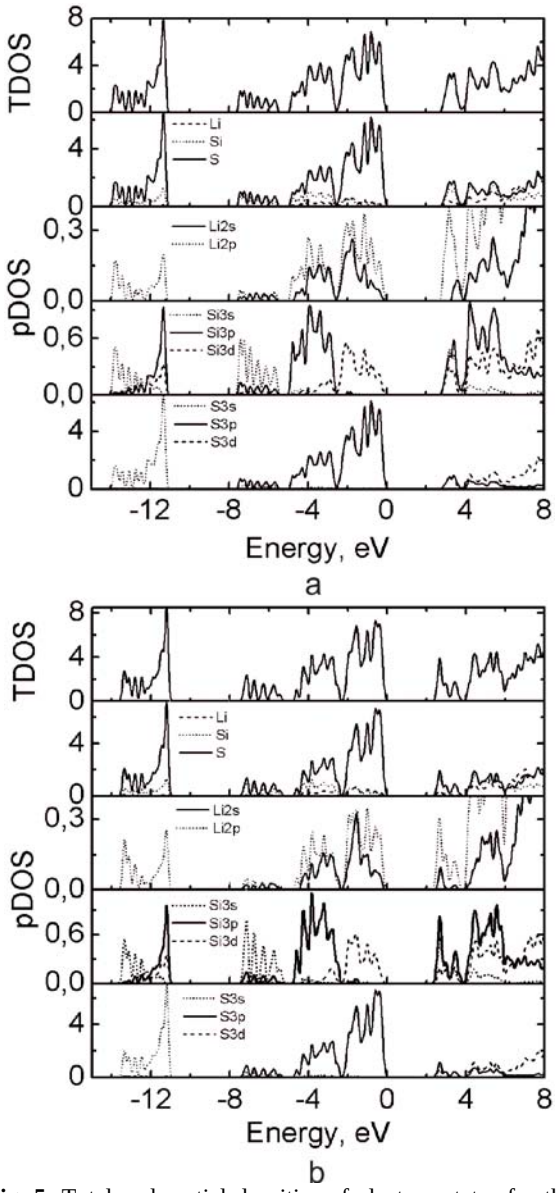

Fig. 5. Total and partial densities of electron states for the equilibrium (*a*) and metastable (*b*) phases in Li_2SiS_3 ($Cmc2_1$).

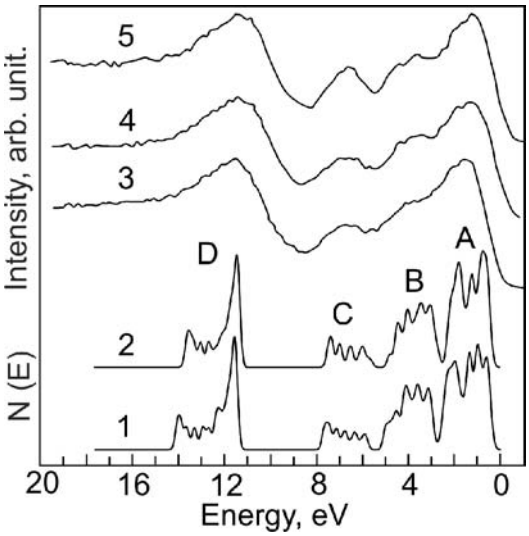

Fig. 6. The calculated total density of electron states $N(E)$, XPS spectra (*3*–*5*) [27] of the equilibrium (*1*, 5), metastable (*2*, *4*), and glassy (*3*) phases in Li_2SiS_3.

electron states with the experimental XPS spectra enables the features of the X-ray photoelectron spectra to be genetically linked with the states of certain symmetry inherent to Si and S atoms, as well as the influence of local environment on the studied valence band structure.

Fig. 6 presents comparison of the experimental X-ray photoelectron spectra (excitation by monochromatic AlK_α radiation with the energy $h\nu$ = 1486.6 eV) for both crystalline phases and glassy Li_2SiS_3 [27] with the calculated total densities of states $N(E)$ in the valence bands of the equilibrium and metastable crystalline phases. It is clearly seen from Fig. 6 that the relative intensities of the main peaks and their energy positions in the XPS spectra of both crystalline phases as well as the glassy phase are in a good agreement with the theoretical curves $N(E)$ of the crystals. Consequently, the observed good agreement of the experimental X-ray photoelectron spectra of the crystals and glass with the corresponding calculated $N(E)$ spectra enables us to conclude that the DFT band calculations give a qualitatively correct picture of Li_2SiS_3 electron structure. Additionally, the similarity of XPS spectra for both Li_2SiS_3 crystals and glass means that the main features of the electron structures of all three phases are determined by the short-range order in the atom arrangement. The analysis of the fine structure of X-ray photoelectron spectra and theoretically calculated local densities of Si *s*-, *p*-, and S *p*-states undoubtedly testifies for a significant mixing of these states and demonstrates the presence of a covalent component in the chemical bond between Si and S atoms in the [SiS_4] coordination tetrahedra that form the infinite chains.

4.2. Spatial distribution of the electron charge

The distribution of electrons in Li_2SiS_3 crystalline phases can be described, at least in the first approximation, by electron charge density mapping. Whereas $\rho(r)$ is a function in the three-dimensional space, the results can be conveniently shown on a plane in the form of electron charge density maps [28]. However, the tetrahedral structure of the short-range order of the crystalline phases in Li_2SiS_3 encumbers 2D mapping. In this case, it is most convenient to present the electron configurations in a separate [SiS_4] tetrahedron in the plane containing two sulfur atoms and one silicon atom. Since [SiS_4] tetrahedra linked in the chain possess two bridging and two non-bridging sulfur atoms, it is reasonable to build two planes: one across the silicon atom and two bridging sulfur atoms and the second one – across the silicon atom and two non-bridging sulfur atoms. The distribution of the valence charge between the silicon ions and the bridging and non-bridging sulfur ions belonging to the same [SiS_4] tetrahedron is illustrated by the electron density maps in Figs 7a and 7b, respectively. The contours of the contribution of the core electrons have a very high concentration near the Si and S atom locations. Comparison of the maps (Figs 7a

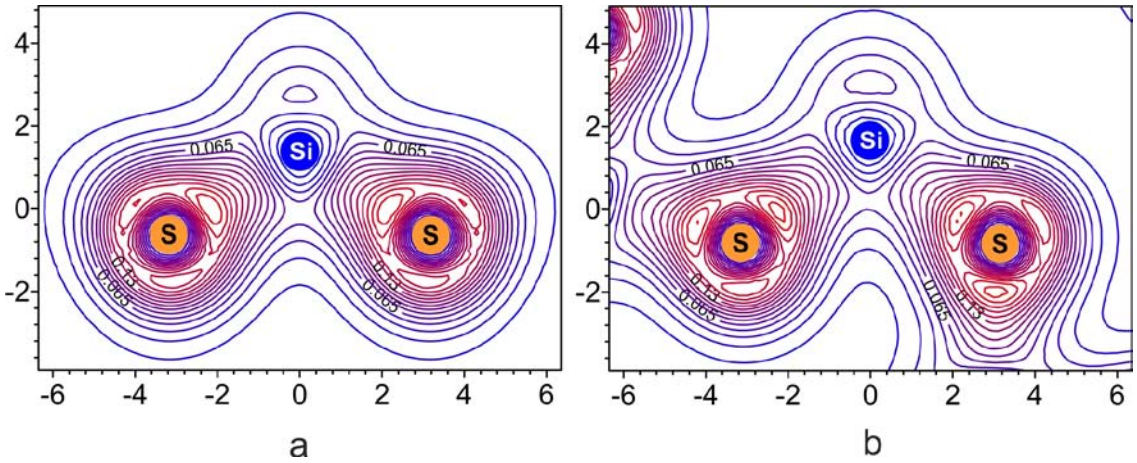

Fig. 7. Spatial distribution of the charge density in the valence band of Li_2SiS_3 in the plane of S–Si–S bond containing: non-bridging (*a*) and bridging (*b*) sulfur atoms.

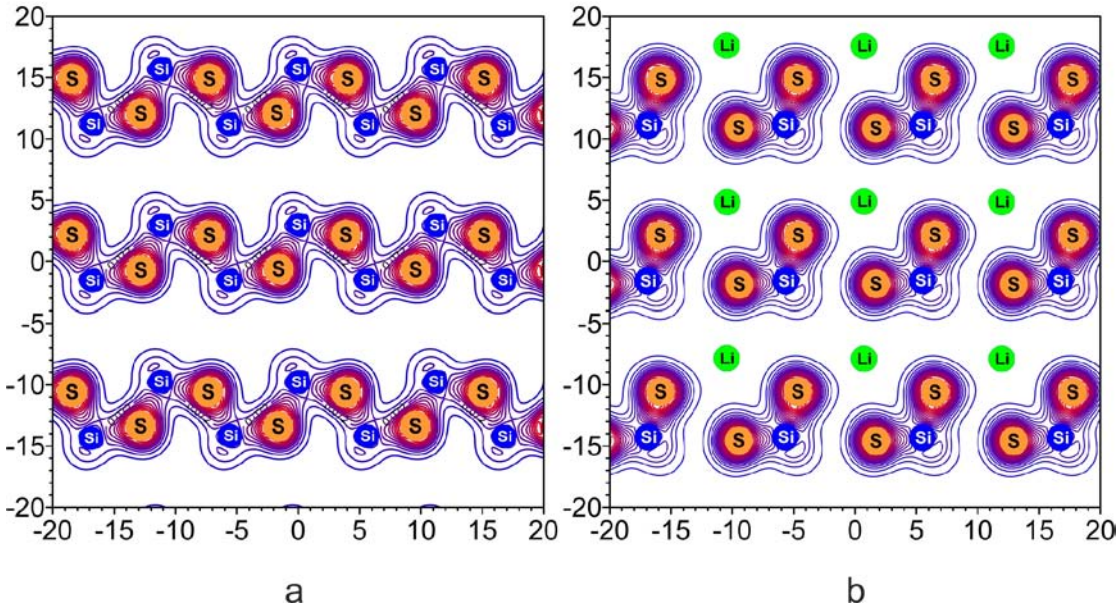

Fig. 8. Maps of the electron density: (*a*) in the plane $(1\bar{1}0)$ built across the silicon atoms and bridging sulfur atoms in a $[SiS_4]$ tetrahedron; (*b*) in the plane passing through the silicon, non-bridging sulfur, and lithium atoms in the Li_2SiS_3 equilibrium phase.

and 7b) shows both planes have common contours of the density ρ(*r*) encompassing sulfur atoms and anions in general as well as sulfur and silicon atoms. The difference consists in the fact that the plane passing through the non-bridging sulfur atoms contains only common contours encompassing sulfur atoms and the same silicon atom. These contours extend from each of the sulfur atom only along one Si–S bond line (Fig. 7a). The plane passing through two non-bridging sulfur atoms (Fig. 7b) contains common contours encompassing the same bridging sulfur atom of one tetrahedron and two silicon atoms belonging to two neighboring tetrahedra.

As a result of interaction between sulfur and silicon atoms, the electron charge is redistributed from the silicon to sulfur atoms along the Si–S bond line, thus providing the covalent component of the chemical binding within $[SiS_4]$ tetrahedra belonging to the same chain. The transfer of a significant part of its valence charge from silicon atoms to sulfur favors hybridization of Si 3*p*-orbitals with S 3*s*-orbitals. Ionic binding is characterized by the increase in charge around the anion and the charge decrease at the covalent bond between ions inside the tetrahedron. In both crystalline phases, anisotropy of the charge density is observed, reflecting the difference in the interaction between S ions belonging to the same chain with the sulfur atoms of neighboring chains. Ions from two different neighboring chains interact extremely weakly (Fig. 8a).

The weak participation of lithium atoms in formation of electron states can be seen from the contour maps in the plane passing through the silicon atoms, non-bridging sulfur, and lithium atoms (Fig. 8b). Their shape clearly shows that contributions of sulfur atoms occupy much wider space than those from silicon and by far wider than those from lithium. The small charge density around Li^+ ions and the presence of channels between the chains with very low charge density along the *c* axis provide the high mobility of lithium ions along these channels and, as a consequence, the high ionic conductivity of both crystalline phases Li_2SiS_3.

5. Conclusions

The band structure of two polymorphic forms of crystalline Li_2SiS_3 superionic conductor was calculated by non-empirical density functional method in the local approximation. This made it possible to elucidate the main features of the electron structure of this compound. Both crystals are indirect-gap superionic semiconductors with the calculated band gap values of 2.82 eV for the equilibrium phase and 2.52 eV for the metastable phase.

The profiles of the total densities of electron states *N*(*E*) for both crystalline phases are similar and correlate with all the features in the experimental XPS spectra of the corresponding crystals. Meanwhile, X-ray photoelectron spectra of the glass and the metastable crystalline phase are quite similar. Therefore, the electron structure of Li_2SiS_3 superionic is determined by the short-range order.

Distribution of the electron density over the unit cell is anisotropic. The electron density maps built for a number of crystallographic planes demonstrate that the ionic conductivity is indeed carried out along the "tunnels" between the infinite chains characterized by the minimum electron density.

References

1. B.T. Ahn and R.A. Huggins, Preparation, structures and conductivities of Li_2SiS_3 phases // *Mat. Res. Bull*. **25**, p. 381-389 (1990).
2. B.T. Ahn and R.A. Huggins, Phase behavior and conductivity of Li_2SiS_3 composition // *Solid State Ionics*, **46**, p. 237-242 (1991).
3. B.T. Ahn and R.A. Huggins, Synthesis and lithium conductivities of Li_2SiS_3 and Li_4SiS_4 // *Mat. Res. Bull.* **24**, p. 889-897 (1989).
4. K. Muruganandam and M. Seshasayee, Structural investigation of Li_2SiS_3 glass using X-ray RDF // *Solid State Communs.* **95**, p. 499-502 (1995).
5. D.L. Price and A.J.G. Ellison, Atomic structure and dynamics of fast-ion conducting glasses // *J. Non-Cryst. Solids*, **177**, p. 293-298 (1994).
6. S.R. Elliott, Isotopic-substitution neutron diffraction as a probe of the structural environment of cations in superionic glasses // *Solid State Ionics*, **105**, p. 39-45 (1998).
7. A. Pradel and M. Ribes, Lithium chalcogenide conductive glasses // *Mat. Chem. Phys.* **23**, p. 121-142 (1989).
8. J.H. Kennedy and Y. Yang, Glass-forming region and structure in SiS_2–Li_2S–Li*x* (*x* = Br, I) // *J. Solid State Chem.* **69**, p. 252-257 (1987).
9. H. Eckert, Z. Zhang and J.H. Kennedy, Glass formation in non-oxide chalcogenide systems. Structural elucidation of Li_2S–SiS_2–LiI solid electrolytes by quantitative ^{29}Si, ^{6}Li and ^{7}Li high resolution solid state NMR methods // *J. Non-Cryst. Solids*, **107**, p. 271-282 (1989).
10. A. Pradel, G. Taillades, M. Ribes and H. Eckert, Eckert H. ^{29}Si NMR structural studies of ionically conductive silicon chalcogenide glasses and model compounds // *J. Non-Cryst. Solids*, **188**, p. 75-86 (1995).
11. A. Pradel and M. Ribes, Electrical properties of lithium conductive silicon sulfide glasses prepared by twin roller quenching // *Solid State Ionics*, **18-19**, p. 351-355 (1986).
12. S. Sahami, S.W. Shea and J.H. Kennedy, Preparation and conductivity measurements of SiS_2-Li_2S-LiBr lithium ion conductive glasses // *J. Electrochem. Soc.* **132**, p. 985-–986 (1985).
13. S. Kondo, K. Takada and Y. Yamamura, New lithium ion conductors based on Li_2S-SiS_2 system // *Solid State Ionics*, **53-56**, p. 1183-1186 (1992).
14. N. Aotani, K. Iwamoto, K. Takada and S. Kondo, Synthesis and electrochemical properties of lithium ion conductive glass, Li_3PO_4–Li_2S–SiS_2 // *Solid State Ionics*, **68**, p. 35-39 (1994).
15. D.I. Bletskan, N.V. Polazhinets and D.V. Chepur, Photoelectric properties of crystalline and glassy $GeSe_2$ // *Fizika i tekhnika poluprov.* **18**, p. 223-228 (1984), in Russian.
16. K.-F. Hesse, Refinement of the crystal structure of lithium polysilicate // *Acta Crystallogr. B*, **33**, p. 901-902 (1977).
17. P. Hohenberg and W. Kohn, Inhomogeneous electron gas // *Phys. Rev. B*, **136**, p. 864-871 (1964).
18. W. Kohn and L.J. Sham, Self-consistent equations including exchange and correlation effects // *Phys. Rev. A*, **140**, p. 1133-1138 (1965).
19. D.M. Ceperley and B.J. Alder, Ground state of the electron gas by a stochastic method // *Phys. Rev. Lett.* **45**, p. 566-569 (1980).
20. J.P. Perdew and A. Zunger, Self-interaction correction to density-functional approximations for many-electron systems // *Phys. Rev. B*, **23**, p. 5048-5079 (1981).
21. J.M. Soler, E. Artacho, J.D. Gale, A. Garcıa, J. Junquera, P. Ordejon and D. Sanchez-Portal, The SIESTA method for ab initio order-N materials simulation // *J. Phys.: Condens. Matter*. **14**, p. 2745-2779 (2002).
22. http://www.icmab.es/siesta-joomla
23. G.B. Bachelet, D.R. Hamann and M. Schlüter, Pseudopotentials that work: From H to Pu // *Phys. Rev. B*, **26**, p. 4199-4228 (1982).
24. C. Hartwigsen, S. Goedecker and J. Hutter, Relativistic separable dual-space Gaussian pseudopotentials from H to Rn // *Phys. Rev. B*, **58**, p. 3641-3662 (1998).
25. D.J. Chadi and M.L. Cohen, Special points in the Brillouin zone // *Phys. Rev. B*, **8**, p. 5747-5753 (1973).
26. H.J. Monkhorst and J.D. Pack, Special points for Brillouin-zone integrations // *Phys. Rev. B*, **13**, p. 5188-5192 (1976).
27. D. Foix, H. Martinez, A. Pradel, M. Ribes and D. Gonbeau, XPS valence band spectra and theoretical calculations for investigations on thiogermanate and thiosilicate glasses // *Chem. Phys.* **323**, p. 606-616 (2006).
28. M.L. Cohen, Electronic charge densities in semiconductors // *Science*, **179**, p. 1189-1195 (1973).